Journal of Applied Physics ARTICLE scitation.org/journal/jap

Comparative performance analysis of lead-free perovskites solar cells by numerical simulation

Cite as: J. Appl. Phys. **131**, 175001 (2022); doi: 10.1063/5.0088099
Submitted: 13 February 2022 · Accepted: 19 April 2022 ·
Published Online: 6 May 2022

Shristy Srivastava,[1] Anand Kumar Singh,[1] Prashant Kumar,[1] and Basudev Pradhan[1,2,a)]

AFFILIATIONS

[1]Department of Energy Engineering, Central University of Jharkhand, Brambe, Ranchi, Jharkhand 835205, India
[2]Centre of Excellence (CoE) in Green and Efficient Energy Technology (GEET), Central University of Jharkhand, Brambe, Ranchi, Jharkhand 835205, India

[a)]**Author to whom correspondence should be addressed:** basudev.pradhan@cuj.ac.in

ABSTRACT

Research of lead-free perovskite solar cells (PSCs) has gained attention with an urgent intent to eliminate toxic lead in perovskite materials. The prime intention of this research is to supplement the current research progress with a comparative analysis of various lead-free PSCs through numerical simulation analysis using solar cell capacitance simulator (SCAPS)-1D software. Lead-based toxicity and instability have been one of the major hurdles in restricting perovskite solar cells from being commercialized. This study caters in substituting the need for toxic lead (Pb)-based PSCs with more efficient Pb-free PSCs. The device simulation is carried out in the *n–i–p* configuration of FTO/[6,6]-phenyl-C61-butyric acid methyl ester/perovskite layer/poly[bis(4-phenyl)(2,4,6-trimethylphenyl)amine/Au using six distinct Pb-free perovskites. The impact of various active layers, including hole and electron transport thicknesses and the concentration of doping on solar device performances, has been minutely probed and optimized. $CsSnI_3$ based PSC shows the best power conversion efficiency of 28.97% among all Pb-free devices. This makes very evident its probability to achieve high-performance Pb-free solar devices experimentally at par with lead-based perovskite solar cells in future research.

I. INTRODUCTION

Perovskite solar cells (PSCs) have experienced a quantum jump in their power conversion efficiency (PCE) in the last few decades owing to their easy manufacturing process, cheaper processing cost, higher absorption coefficient, lower surface recombination rates, and comparatively high efficiency.[1–3] It has escalated from 3.8% (2009) to 25.6% until present in single-junction configurations, which has its value approaching the crystalline-Si based solar devices at 26.7%.[4,5] The hybrid organic–inorganic perovskites have unlocked new routes toward more efficient light-harvesting materials. Owing to tunable frequency, these solar devices can be very effective in absorbing distinct light frequencies in different layers that can improve their PCEs, unlike conventional solar cells. Despite this, Pb-based perovskites face two prominent challenges: (a) poor stability—tackled by enhanced device engineering along with the utilization of 2D perovskites and encapsulation and (b) high toxicity—a matter of concern on an environmental level. Non-toxic Pb-free perovskites are also being considered as another alternative.[6] These Pb-free materials will have a huge demand in the solar photovoltaics market, which will ease the commercialization of PSCs if they have good device performance. Ideally, lead-free active materials when utilized as light absorbing layers in devices should have lower toxicity, higher coefficient of absorption, lower exciton-binding, narrower direct bandgaps, and high mobilities. Perovskites in the form of double perovskites, some Sn/Ge-based halides, and also some Bi/Sb-based halides with perovskite-like structures show engrossing properties and are least-toxicity materials. Until 2020, the highest efficiency so far achieved for Sn-based perovskites has been around 13.24%.[7]

In these Pb-free perovskite materials, comparatively, only Sn-based PSCs have shown very promising performance. In Sn (tin)-based PSCs, certain characteristics like low air stability due to sudden oxidation of Sn^{2+} resulting in higher recombination losses, smaller energy available for vacancy formation, higher intrinsic density of carrier, etc., sums up to poor cell performance in comparison to their corresponding Pb-based analogues. The weaker anti-bonding coupling of Sn-5s and I-5p in $FASnI_3$ [FA = $CH(NH_2)_2$] is not as strong as in $CsSnI_3$ and $MASnI_3$ (methyl

ammonium tin iodide) because of the larger FA ion size. This is why there is an elevation in the formation energies in the case of Sn-vacancies.[8,9] According to the demonstration of Milot *et al.* $FASnI_3$ exhibited higher charge-carrier mobility in addition to lower Auger and stronger radiative recombination rate constants, which is similar to GaAs.[10] A study involving bandgap engineering reported a PCE of 5.73% for Pb-free perovskite material of $CH_3NH_3SnI_{3-x}Br_x$.[11] Lee *et al.* achieved a PCE of 4.8% by fabricating $FASnI_3$ combined with SnF_2−pyrazine complex to slow down the crystallization process.[12] Kumar *et al.* worked on the $CsSnI_3$ absorber layer based PSC incorporating vacancy modulation, which showed a PCE of 2.02%, and the experiment was performed in a nitrogen-filled glovebox due to material instability.[13] Zhao *et al.* got a maximum PCE of 8.12% for the $FA_{0.75}MA_{0.25}SnI_3$-based cell and an open-circuit voltage of 0.61 V by optimizing the ratio of FA and MA cations.[14] Abdelaziz *et al.* used SCAPS software to extensively study the impact of thickness, defect density, and doping on the device performance of $[HC(NH_2)_2–SnI_3–FASnI_3]$ based perovskite solar cell. The optimized cell exhibited PCE of 14.03%, V_{OC} as 0.92 V, J_{SC} as 22.65 mA/cm^2, and FF of 67.74%.[15] Neol *et al.* fabricated Pb-free device with $CH_3NH_3SnI_3$ as the absorber material in the FTO/c-TiO_2/mp-TiO_2/$CH_3NH_3SnI_3$/Spiro-OMeTAD/Au device configuration that exhibited an efficiency of 6%.[16] It was observed that Sn^{2+} in Pb-free light absorbing material changed to Sn^{4+} under ambient conditions to achieve a more stabilized state. As a result, SnO_2 and methyl ammonium iodide (MAI) are formed after the breaking of charge neutrality in the perovskite. So, stability is a serious concern when it comes to Pb-free Sn-based perovskites. However, tin-based perovskites can use the same technologies to address the stability issues. When Pb-free perovskite candidates are concerned, which have already achieved PCE of 13.24% by the partial substitution of FA with EA cation which also decreases the trap density by one order magnitude.[7] V_{OC} in the range of 0.8–1.00 V can be achieved if the Sn^{4+} oxidation issue is completely addressed and the photocarrier recombination rates are lowered down to the levels of the $APbI_3$(A=Li, Na, K, Rb, and Cs) materials. This could assist to drastically enhance the PCE above 15% and help them to come up as suitable Pb-free contenders in the coming future.[17]

In the Pb-free perovskites field, many studies are being done to obtain clues about their characteristics, avenues, and applicability. The prime hurdle associated with Pb-free perovskites is (i) high-efficiency but poor stability (Sn^{2+}-based) or (ii) decent stability but low performance (Sn^{4+}/Sb/Bi-based, etc.). A Pb-free perovskite with good optical and electrical characteristics needs to be explored for an optimized balance between stability and performance. Along with the experimental work, simulation also has a crucial role in investigating distinct properties of the materials and their corresponding performance parameters. This study aims at studying the material properties in relation to the performance parameters, comparing multiple materials with the help of theoretical analysis by designing a device model. Here, a comparative examination of different Pb-free active materials in the same configuration is executed, which helps us to understand the distinguishing performance, their effect on performance parameters, and further work for achieving high efficiencies for Pb-free perovskites.

II. DEVICE ARCHITECTURE AND SIMULATION METHODOLOGY

A. Device architecture and modelling

In this modelling analysis, an in-depth study has been performed on different Pb-free PSCs using the SCAPS-1D software. The Pb-free perovskites have obtained significance in the last few years due to their non-toxicity in contrast to toxic Pb- based perovskites. The device configuration considered here is one of the prime aspects of the numerical analysis being executed. This simulation is done in the *n–i–p* configuration of fluorine-doped tin oxide (FTO)/[6,6]-phenyl-C61-butyric acid methyl ester (PCBM)/perovskite layer/poly[bis(4-phenyl)(2,4,6-trimethylphenyl)amine (PTAA)/Au, which is depicted in Fig. 1(a). PCBM and PTAA, over here have been used as the ETL and HTL, respectively. Different Pb-free perovskite layers such as $FASnI_3$ (1.41 eV), $CsSnI_3$ (1.3 eV), Cs_2AgBiI_6 (1.6 eV), $CsSnCl_3$ (1.52 eV), Cs_2TiBr_6 (1.8 eV), and $MASnI_3$ (1.35 eV) are used as active layer, sandwiched between ETL and HTL. FTO performs in a twofold way in serving as a front contact and transparent conductive oxide through which light passes. Au acts as a back metal contact. In this analysis, the prime intent has been subjected to an in-depth behavioral study of various halide based Pb-free perovskites in a similar configuration. This will demonstrate the outcome of the perovskite properties on PSC performance and will also help in determining the Pb-free perovskite that performs the best on this particular configuration. Figure 1(b) represents the band diagram showing the flow of carriers in the device comprising of all the active materials taken here, along with contacts and carrier transport layers. The properties of materials such as energy bandgap, layer thickness, doping concentration, charge carrier mobilities, thermal velocities, electron affinity, dielectric permittivity, conduction band (CB), and valance band (VB) effective density of states are required for the simulation work, which is also mentioned in Table I.

B. SCAPS-1D simulation methodology

The simulation and the calculations performed in the SCAPS-1D software are primarily based on three basic equations, namely, Poisson's equation, electron continuity equation, and hole continuity equation, respectively.[18,19] This is a 1D solar cell simulation software that has been developed at the Department of Electronics and Information Systems (ELIS) of University of Gent, Belgium.[20] In this software, the designed model can simulate a maximum of seven semi-conductor layers, and besides this, it gives the flexibility of grading and tuning different properties as in energy bandgap, electron affinity, defects, doping, interfacial properties, etc., for each of the layers. The software is feasible for simulating different solar device structures from crystalline amorphous to even organic and perovskite solar cells (PSCs). The spectral condition under which the simulation has been performed is AM 1.5G 1 sun spectrum. The properties of each of the ETL, HTL, and the Pb-free perovskite layers have been varied to achieve an optimized result. The thickness and doping concentration has been differed within a feasible range to study the plot type obtained with the changing values. This makes it very simple and quite precise to obtain optimum values of each of the layers, which further helps in

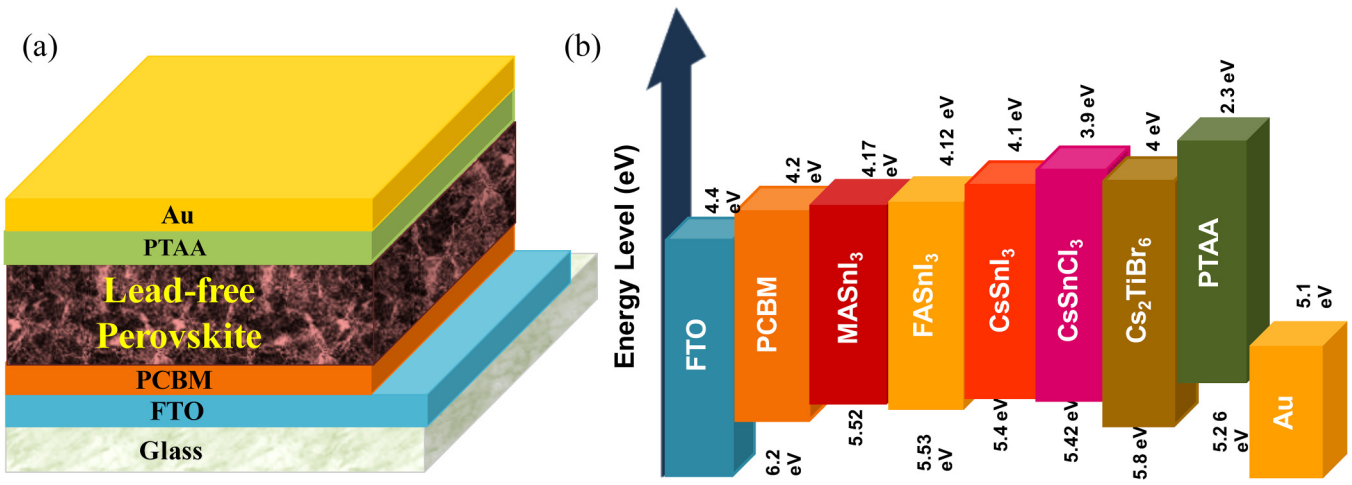

FIG. 1. (a) Schematic structure of the simulated PSCs, (b) energy-band diagram of different Pb-free perovskites with ETL and HTL.

obtaining the optimized performing solar cell. This is done for all the Pb-free perovskites taken into account in this study, which helps in understanding the performance and effect of properties for each material. The mathematical equations that are crucial in the numerical simulation analysis are described below. For semiconductors, Poisson's equation is given by

$$\frac{d^2\psi(x)}{dx^2} = \frac{q}{\varepsilon}\,(n - p + N_A - N_D), \tag{1}$$

where ε is the permittivity of the semiconductor, N_A represents the acceptor concentration, N_D is the donor concentration, and ψ resembles the electrostatic potential.

Now, the electron and hole continuity equations for a semiconductor are given by

Electron continuity equation

$$\frac{\partial J_n(x)}{\partial x} - q\frac{\partial n}{\partial t} = +qR. \tag{2}$$

Hole continuity equation

$$\frac{\partial J_p(x)}{\partial x} + q\frac{\partial p}{\partial t} = -qR. \tag{3}$$

In the above Eqs. (2) and (3), J_n is the current density for electrons, J_P is symbolic of the current density for holes, and R represents the rate of carrier recombination.

Another very essential set of equations is the drift–diffusion current relations that are given by the continuity equations shown

TABLE I. Main physical properties for various layers of the Pb-free perovskite devices.[15,19,21–28] X, thickness of the material; E_g, bandgap; χ, electron affinity; ε_r, dielectric affinity; N_C, CB effective density of states; N_V, VB effective density of states; V_n, electron thermal velocity; V_h, hole thermal velocity; μ_n, electron mobility; μ_h, hole mobility; N_D, donor density; and N_A, acceptor density.

Material properties	PTAA	PCBM	FTO	$FASnI_3$	$CsSnI_3$	Cs_2BiAgI_6	$CsSnCl_3$	Cs_2TiBr_6	$MASnI_3$
X (nm)	Varied	Varied	100	Varied	Varied	Varied	Varied	varied	varied
E_g (eV)	2.96	2.00	3.5	1.41	1.3	1.6	1.52	1.8	1.35
χ (eV)	3.5	3.9	4.0	3.52	3.6	3.9	3.9	3.9	4.17
ε_r	9	4	9	8.2	9.93	6.5	29.4	6.5	6.5
N_C (cm^{-3})	1×10^{21}	1×10^{21}	2.2×10^{18}	1×10^{18}	1×10^{19}	1×10^{19}	1×10^{19}	1×10^{19}	1×10^{18}
N_V (cm^{-3})	1×10^{21}	2×10^{20}	1.8×10^{19}	1×10^{18}	1×10^{18}	1×10^{19}	1×10^{19}	1×10^{19}	1×10^{19}
V_n (cm/s)	1×10^{7}	1×10^{7}	1×10^{7}	1×10^{7}	1×10^{7}	1×10^{7}	1×10^{7}	1×10^{7}	1×10^{7}
V_h (cm/s)	1×10^{7}	1×10^{7}	1×10^{7}	1×10^{7}	1×10^{7}	1×10^{7}	1×10^{7}	1×10^{7}	1×10^{7}
μ_n (cm^2/V s)	1×10^{-3}	1×10^{-2}	20	22	1.5×10^{3}	2	2	2	1.6
μ_h (cm^2/V s)	1×10^{-3}	1×10^{-2}	10	22	5.85×10^{2}	2	2	2	1.6
N_D (cm^{-3})	…	Varied	1×10^{17}	…	…	…	…	Varied	…
N_A (cm^{-3})	Varied	…	…	Varied	Varied	Varied	Varied	…	Varied

in (4) and (5). There are two ways in which current is conducted in a semiconductor. First and foremost, diffusion current is produced due to the difference in carrier concentration on either side of the device (concentration gradient). Second, the drift current that is build up due to the drift of minority charge carriers under the electric field

$$J_n = qn\mu_n E + qD_n \frac{\partial n}{\partial x}, \tag{4}$$

$$J_p = qp\mu_p E - qD_p \frac{\partial p}{\partial x}, \tag{5}$$

where D_p is the diffusion coefficient for holes and D_n is the diffusion coefficient for electrons. E represents the electric field, q is the quantity of charge, n and p represent the number of electrons and holes. μ_n and μ_p represent the mobility of electrons and holes, respectively. Other relations that govern the performance parameters are as follows.

For open circuit voltage,

$$V_{OC} = \frac{nkT}{q} \ln\left(\frac{J_{SC}}{J_S} + 1\right), \tag{6}$$

where J_{SC} is the short circuit current density (or, light generated current) and J_S is the reverse saturation current.

For short circuit current density,

$$J_{SC} = -J_L. \tag{7}$$

Fill factor and efficiency are given by the relation

$$FF = \frac{P_{max}}{J_{SC} V_{OC}}, \tag{8}$$

$$\eta(PCE) = \frac{P_{max}}{P_{in}} = \frac{FF \times J_{SC} \times V_{OC}}{P_{in}}. \tag{9}$$

For better device performance, light absorbing layer of solar cells has a major role. In this simulation, different Pb-free perovskite materials will be used to find out the best configuration to achieve higher performances. Major attention is given to optimize different parameters in a way through which we can get a clear insight of device performances. The absorption spectra of the perovskite materials used in this simulation are shown in Fig. 2, which will help us to understand the thickness dependence, optical absorption index (extinction factor) of the material that affects the carrier generation distribution and electrical internal resistance of the film. Table I shows the different layer parameters that have been used for this simulation process. Some values have been derived from the already published papers, while others have been optimized within the feasible limit after studying the impacts of different structural properties on the device performance.

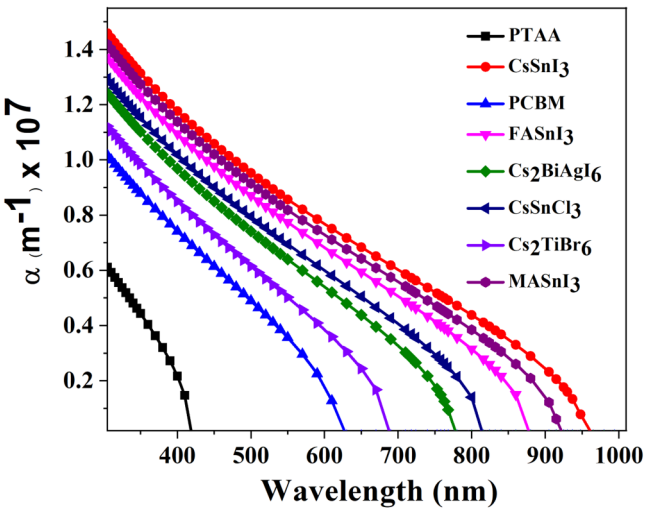

FIG. 2. Plot showing a variation of absorption coefficient with wavelength for different materials used in this work.

III. RESULTS AND DISCUSSION

The simulations of Pb-free PSCs were executed on tabulated property parameters obtained from different research works. Different Pb-free perovskites have been utilized as an absorber layer in the device structure of FTO/PCBM/perovskite layer/PTAA/Au while keeping all the other parameters the same, except the light absorbing layer which has been varied between different Pb-free perovskites materials. Using this configuration, the device models have been simulated to obtain an optimized result for each case. To obtain optimized device performance, thickness and doping concentration of the active absorber layers were varied. Perovskite layer properties determine the device quality which solely depends on the carrier diffusion lengths, charge carrier mobility values for both electrons and holes, and carrier lifetime. The perovskite thickness has been varied to observe the changes in device performances. The active layer thickness was varied from 100 to 1000 nm keeping other parameters, including temperature, constant for the sake of comparative analysis. The impact of thickness on device performance for different Pb-free active layers is illustrated in Fig. 3. With the increase in thickness, V_{OC} decreases or almost remains the same in most of the cases as shown in Fig. 3(a). An abnormal behavior is noticed for $CsSnCl_3$ where an increase in V_{OC} is observed first, followed by a constant nature. The reason behind this could be accredited to interfacial kinetics owing to band-energy mismatch. The nature of curves obtained for short-circuit current density (J_{SC}) and efficiency (η) vs thickness is nearly the same as depicted in Figs. 3(b) and 3(d). As the thickness of the absorber increases, J_{SC} and η values increase, reach an optimum value, and decrease slowly as the layer thickness increases for all perovskite materials, but the optimum thickness in which PCE reaches the highest value is different for different perovskite materials, which varies between 300 and 500 nm under this configuration. This trend is due to the fact that as active layer thickness

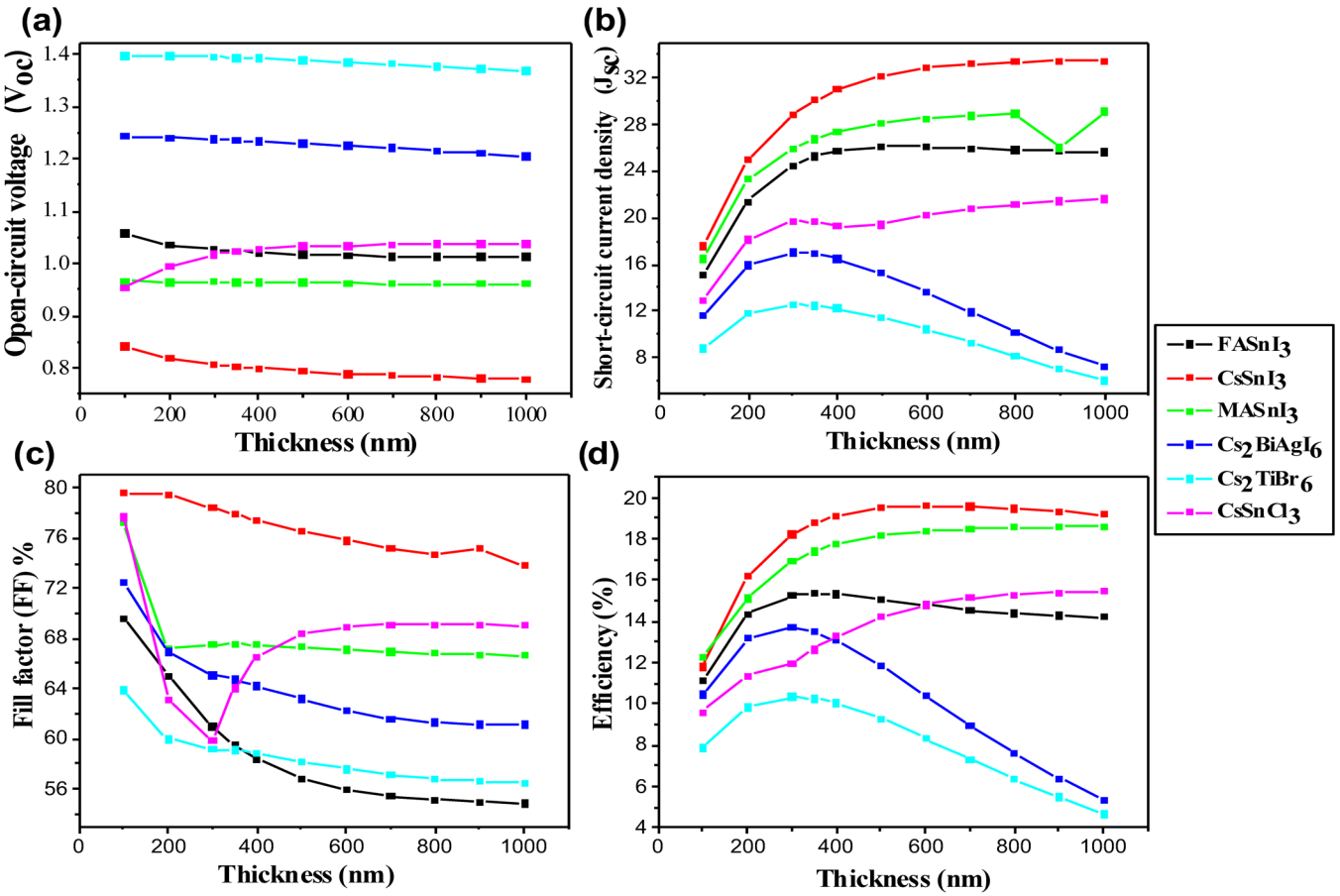

FIG. 3. Variation of solar cell performance parameter, (a) open circuit voltage (V_{OC}), (b) short-circuit current density (J_{SC}), (c) fill factor (*FF*), and (d) efficiency (η) with Pb-free perovskites layer thickness.

increases, more light absorption occurs in the device, which implies more charge carrier generation and higher light generated current that consequently leads to higher J_{SC} and efficiency.[29] Further increase in thickness may exceed the diffusion length of these materials, causing the recombination rate of charge carriers to increase, which eventually leads to an increased saturation current, hence decreased V_{OC} and also $J_{SC,}$ which ultimately reduces efficiency. But, in some specific materials, such as $FASnI_3$, Cs_2BiAgI_6, and $Cs_2TiBr_{6,}$ the values increase to a certain point and then decrease very fast with an increase in thickness. In these materials, after a definite point, an increase in active layer thickness results in higher series resistance and back contact recombination, which, in turn, reduces J_{SC} and η. The fill factor plot [Fig. 3(c)] shows a decrease in value as the perovskite thickness increases and this could be described by the *FF* dependency on perovskite layer thickness, since *FF* signifies how easily electron–hole pairs move through the device without recombination. With increased perovskite layer thickness, charge pathway resistance should increase leading to a decrease in *FF*. On the contrary, recombination in Pb-free perovskite occurred because of a reduced charge carrier [electron (t_n) and hole (t_p)] lifetime, which does not allow a sufficient period for the charge carrier to develop CB at Pb-free perovskite.[21] Certain abnormality of *FF* in case $CsSnCl_3$ with an increase in active layer thickness was also observed.

The dopant concentration of perovskite materials plays a very significant role in determining the electrical behavior of the solar cell which has a major impact on the solar cell performance. The variation of doping for all lead-free perovskites has been plotted together as the function of solar cell performance parameters. The doping of the active layer has been varied from 1×10^{14} to 5×10^{20} cm^{-3}. The rest of the properties are kept constant and the impact has been studied by comparing the behavior of various materials. Figure 4 shows an impact on different solar cell parameters due to the variation of doping concentration in different absorber materials. The V_{OC} of all perovskite materials increases steadily with the increase of doping concentration as in Fig. 4(a), reverse saturation current decreases with the increase in doping concentration, which leads to the increase in open circuit

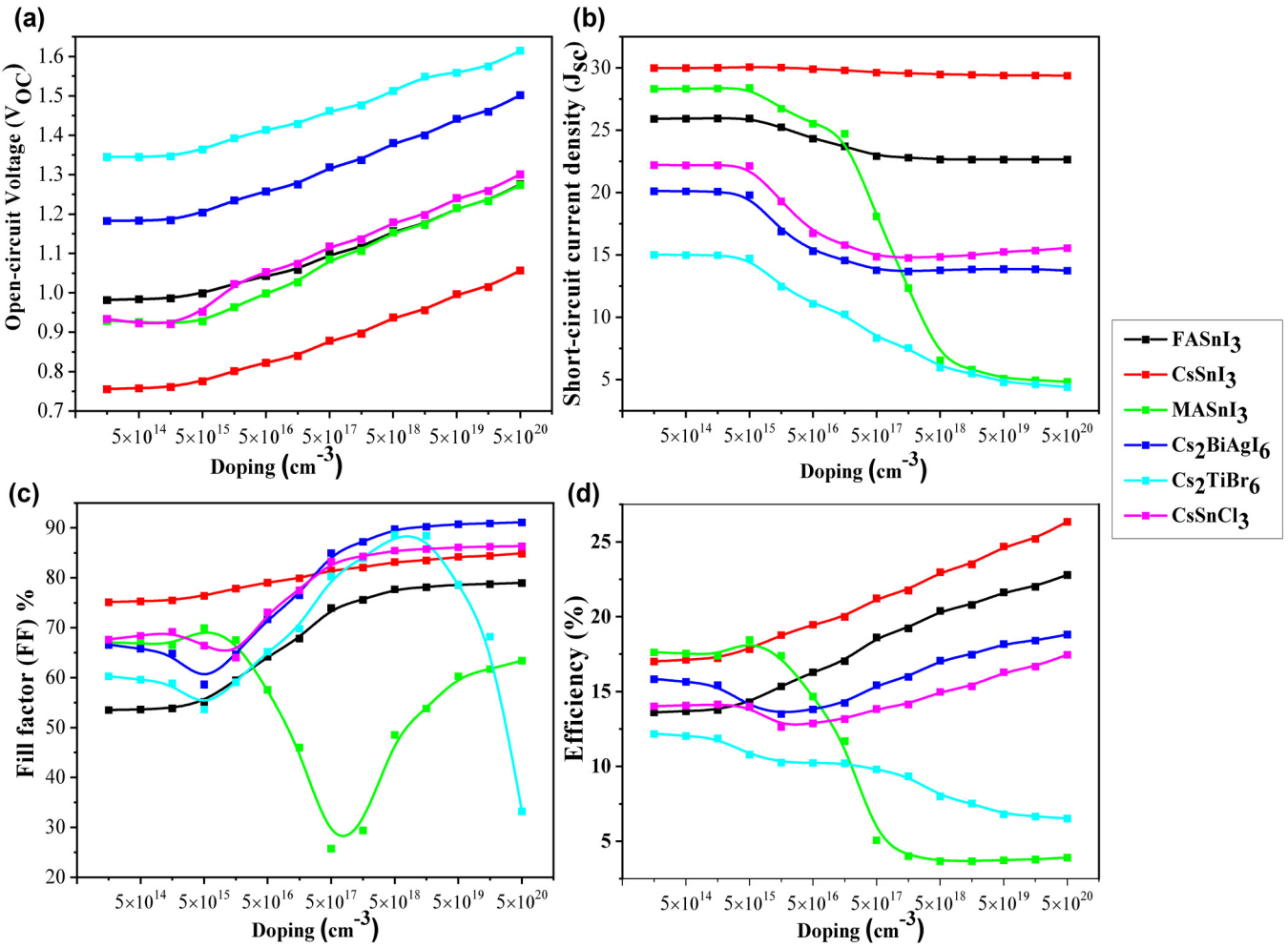

FIG. 4. Impact of doping density of different Pb-free perovskites on performance parameter, (a) open circuit voltage (V_{OC}), (b) short-circuit current density (J_{SC}), (c) fill factor (*FF*), and (d) efficiency (η).

voltage.[30,31] On that hand, built-in potential (V_{bi}) as shown in the Eq. (10) is strongly dependent on the doping concentration

$$V_{bi} = \frac{kT}{q}\ln\frac{N_A N_D}{n_i^2}, \tag{10}$$

where k is Boltzmann's constant, T is the temperature, q is the electron charge, n_i is the intrinsic concentration, N_D is donor doping concentration, and N_A is the acceptor doping concentration. As the doping concentration increases, V_{bi} also increases, which gets reflected in V_{OC}. The maximum V_{OC} is observed for a Cs_2TiBr_6 (1.8 eV) based device, whereas the lowest for a $CsSnI_3$ (1.3 eV) based cell; others follow the trend that is adequate because open circuit voltage increases with the increasing bandgap. The short circuit current densities of all lead-free perovskites decrease with an increase in doping concentration as depicted in Fig. 4(b). Lower doping concentration serves for higher carrier collection due to a wider depletion region; increased doping levels lead to a narrow charge collection region, hence, reduced J_{SC} at higher doping. The higher bandgap materials have lower J_{SC} values and vice versa in the V_{OC} curve trend. In most perovskites, the *FF* is observed to first increase as the doping concentration increases, and then, it remains almost constant, whereas an abnormality *FF* curve is observed for $MASnI_3$ and Cs_2TiBr_6 as represented in Fig. 4(c). The efficiency of most materials is seen to increase with increasing doping values, while a decrease in η is observed in $MASnI_3$ and Cs_2TiBr_6 while for Cs_2BiAgI_6, initially, it decreases and then increases slowly as shown in Fig. 4(d). The nature obtained in this case is highly dependent on the behavior each material reflects in the previous three performance parameters; hence, a decrease in η of $MASnI_3$ and Cs_2TiBr_6 due to a decrease in *FF* and J_{SC}. The explanation for such nature of *FF* and η could be due to a decreased resistance with

an easy charge carrier pathway because of increased doping concentration.

The doping concentration and thickness of PTAA have negligibly impacted the performance parameters of all the perovskites. As per Fig. 5(a), initially, there is a negligible decrease in η with an increase in the thickness of HTL, which later on becomes constant for all PSCs, implying no major influence of the HTL thickness on PCE. On the contrary, an increase in PCE is seen as the doping of HTL increases (the highest rate of increase being observed for $FASnI_3$), whereas the value slightly decreases at very high HTL doping levels for $CsSnI_3$ devices as in Fig. 5(b). ETL contributes in modifying the interfacial layer, controlling charge recombination rates, and also synchronizing interfacial energy levels. The efficiency of all perovskite-based devices reduces with an increase in the ETL layer thickness which is given in Fig. 5(c). Figure 5(d) shows that efficiency slowly increases with an increase in the ETL doping concentration. A continuous rise in PCE is clearly seen as the ETL doping concentration increases, except in $CsSnI_3$, which after $10^{19}\,cm^{-3}$ of doping concentration observed reduction in PCE, whereas for $MASnI_3$, efficiency continues to be constant after $10^{17}\,cm^{-3}$ doping concentration. Overall, the PCE rises slowly as the HTL and ETL doping concentration increases, but in the case of most perovskites, the values remain constant. As the donor concentration increases, the conductivity also increases, which reduces device J_{SC} and it maintains a constant value. After a certain limit of donor concentration, the solar cell performance parameters remain unchanged due to the Moss–Burstein effect.[32] The increase of HTL and ETL doping levels also enhances the interface electric field between the transport layers; this enhanced electric potential contributes to the separation of the excitons with a lower recombination rate, and thus, the overall performance of the device is increased. Alternatively, moderate doping is also needed, whereas heavy doping leads to increased recombination and the perovskite's semi-conductive nature changes to metallic, which obstructs the carrier transport mechanism.[33]

The J–V characteristics and quantum efficiency curve in light conditions for various lead-free perovskite materials have been plotted under optimized conditions as shown in Figs. 6(a) and 6(b), respectively. All the devices exhibit very good J–V characteristics. $CsSnI_3$ possessing the least bandgap has the widest absorption spectrum and Cs_2TiBr_6 has the narrowest, the rest of the materials falling in order. As per QE plots obtained, the devices

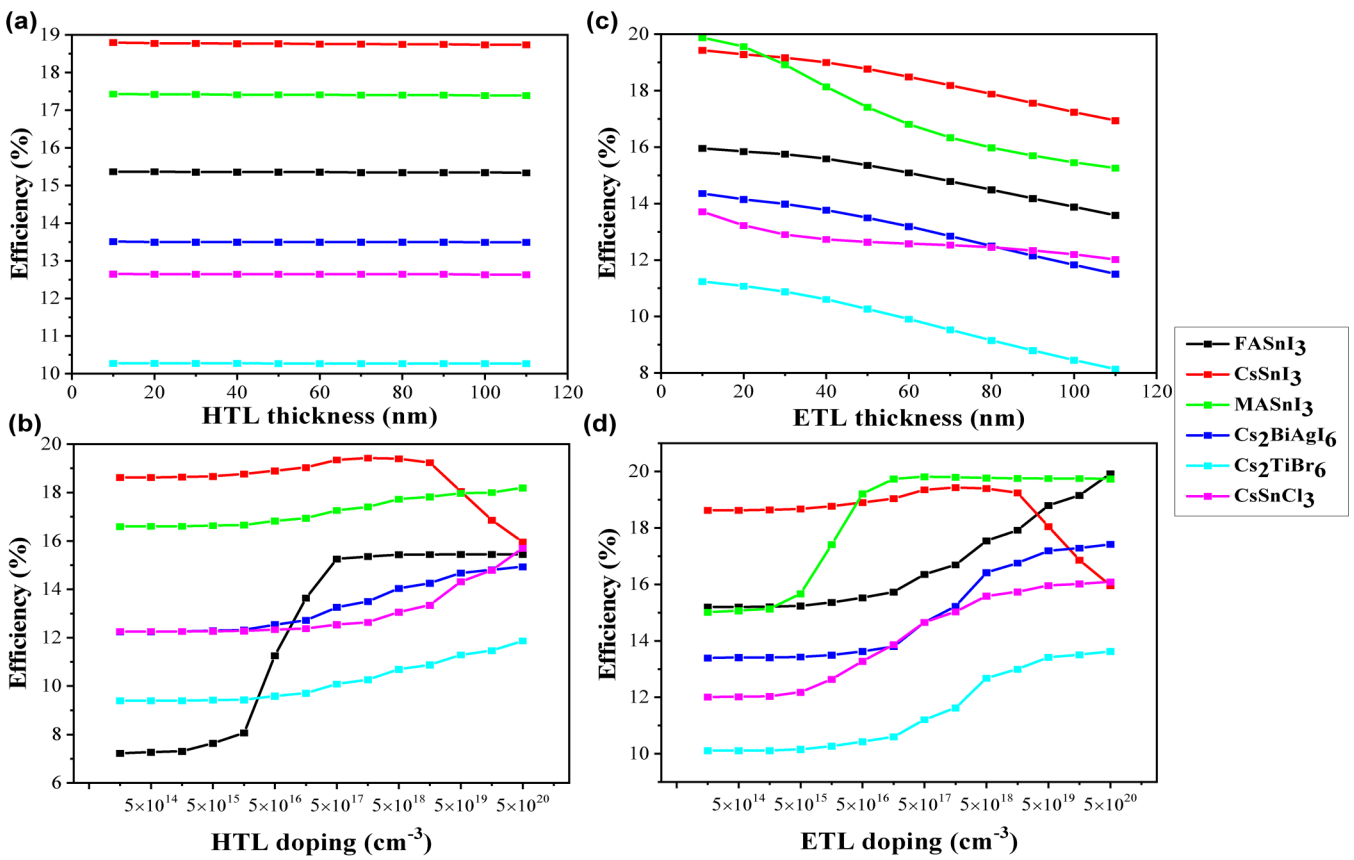

FIG. 5. Variation of the efficiency of different Pb-free perovskites solar cells with (a) hole transport layer thickness (HTL), (b) HTL doping density, (c) electron transport layer thickness (ETL), and (d) ETL doping density.

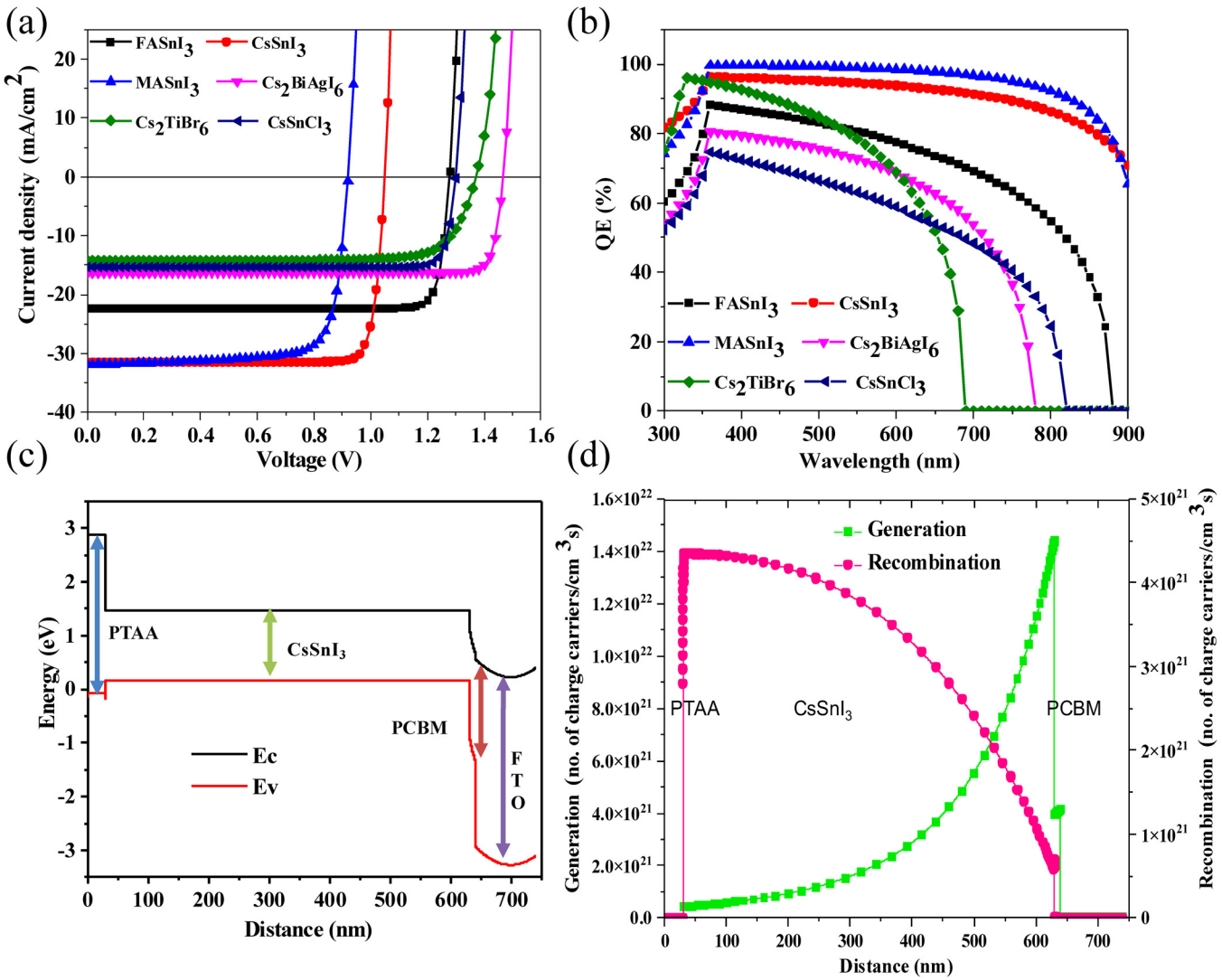

FIG. 6. (a) *J–V* characteristics and (b) corresponding QE spectra of PSCs with different Pb- free perovskites. (c) Energy band structure diagram of the $CsSnI_3$ based perovskite solar cell, (d) generation recombination profile of the $CsSnI_3$ based PSC.

with the best QE are $MASnI_3$ and $CsSnI_3$ based cells, with minimum losses of energy and maximum QE obtained at ~75% and ~82%, respectively. The QE values at the low wavelength region for these materials suggest that the electrons due to the energy photons are efficiently generated and collected. On the contrary, it also reflected that the top surface is well passivated. In the higher wavelength region, a higher QE is seen for $MASnI_3$ and $CsSnI_3$ based cells, which eventually leads to higher values of short circuit current. Table II represents the performance parameters obtained for six different Pb-free perovskites based solar cells, when simulated under AM 1.5G 1 sun spec, 300 K temperature, keeping other performing conditions the same. Among all

TABLE II. Performance parameters for optimized devices with various Pb-free perovskites.

Pb-free perovskite	V_{OC} (V)	J_{SC} (mA/cm^2)	FF (%)	Efficiency (%)
$FASnI_3$	1.279	22.31	89.65	25.58
$CsSnCl_3$	1.300	15.34	89.90	17.93
$MASnI_3$	0.921	31.92	77.76	22.86
Cs_2BiAgI_6	1.468	16.32	90.78	21.75
Cs_2TiBr_6	1.371	14.21	79.61	15.50
$CsSnI_3$	1.048	31.50	87.77	28.97

simulated devices, Cs_2BiAgI_6 shows the highest V_{OC} of 1.468 V, whereas $MASnI_3$ shows the lowest V_{OC} of 0.921 V. The device with $MASnI_3$ shows the highest of J_{SC} 31.92 mA/cm^2. $CsSnCl_3$ and $FASnI_3$ based devices show higher *FF* as compared to other devices. Figure 6(c) depicts the band diagram of $CsSnI_3$ based PSC with PTAA and PCBM as HTL and ETL, respectively, from SCAPS-1D. Overall, the $CsSnI_3$ based device shows the highest PCE of 28.97%, V_{OC} of 1.048 V, J_{SC} of 31.50 mA/cm^2 and *FF* of 87.77% among the other perovskite-based solar cells, which is so far the highest reported value in this configuration by any simulation method. Previously, Shafi *et al.* simulated perovskite solar cells in back contact/$MASnBr_3$/CdS/ZnO/front contact structure.[34] They observed that as the buffer layer thickness was increased from 1.0 to 3.0 μm, then the PCE was increased from 16.17% to 20.81%, while when the temperature was increased from 290 to 330 K, the PCE was seen to reduce from 19.99% to 17.31%. Another study by Lin *et al.* simulated using AMPS-1D software, which used B-γ-$CsSnI_3$ as an all-inorganic Pb-free active layer, compared the performance of the device with different electron transport layers. The study concluded that on the cell architecture of FTO/(TiO_2/ZnO/SnO_2/GaN/C_{60}/PCBM)/B-γ-$CsSnI_3$/spiro-OMeTAD, the device with TiO_2 as ETL exhibited the best performance of 20.2%.[35] Hussain *et al.* made a comparison between a double perovskite-based PSC and Pb-based PSC ($MAPbI_3$) showed that the Pb-free double perovskite with the device architecture FTO/TiO_2/$(FA)_2BiCuI6$/spiro-MeOTAD/Au showed optimized PCE of 24.98% at 300 nm by using SCAPS-1D simulation.[36]

For a further deeper understanding of this result, we have tried to calculate the ideality factor from the dark characteristics. The value of ideality factor for each perovskite solar cell using different perovskite materials was calculated by fitting the diode equation and almost ideal diode nature was observed in the case of $CsSnI_3$, $FASnI_3$, $CsSnCl_3$ based devices with ideality factor value of around 1.02, 1.05, and 1.07, respectively. Ideality factor values remained 1.4, 1.5, and 1.7 in the case of $MASnI_3$, Cs_2BiAgI_6, and Cs_2TiBr_6, respectively, exhibiting a slightly higher value from the ideal trend. All the devices show the reverse saturation current density in the order of 10^{-16} mA/cm^2. Perovskite solar cell with $CsSnI_3$ shows the lowest ideality factor compared to other perovskite-based devices in the same device configuration. The high performance of the $CsSnI_3$ based solar cell would be due to the small optical bandgap of perovskite material combined with a higher coefficient of absorption and lower exciton energy. Simultaneously, it also shows high electron dimensionality,[37] relatively high intrinsic or thermodynamic stability.[38] It was also observed from the generation and recombination depth profile of the charge carrier that the carrier generation is higher for PCBM and perovskite interface and carrier recombination is lower, while for PTAA and perovskite interface, generation is low and recombination is high as shown in Fig. 6(d). Therefore, from this study, it is evident that $CsSnI_3$ based Pb-free PSCs can definitely be the best alternative to the Pb-based PSCs.

IV. CONCLUSION

Concisely, an exhaustive performance study of various Pb-free PSCs has been investigated by numerical simulation on SCAPS-1D. As per WHO (World Health Organization), lead has been declared as one of the most toxic elements that needs to be eliminated deliberately from the devices. Consequently, better substitutes for lead have been found, thus making Pb-free materials more environmentally sustainable. In PSCs, we are mainly looking into the ionic form of lead, which can create great damage on the ground level. However, this study guides us in finding a better alternative for commercialization in the form of Pb-free PSCs with high efficiency. A detailed study has been executed to investigate the influence of various perovskite properties, doping, thickness, and their impact on the PCE on a similar device configuration, having HTL as PTAA and ETL as PCBM. We have optimized material properties such as doping concentration, active material thickness, as well as ETM and HTM for further improvement of performance. Among all Pb-free perovskite devices, $CsSnI_3$ based device exhibits the highest PCE of 28.97% with V_{OC} of 1.048 V, J_{SC} of 31.50 mA/cm^2, and *FF* of 87.77%. So, based on our simulation study, it is evident that Pb-free PSCs definitely guide the scientific community for further exploration toward experimental realization in lead-free perovskite solar cells in the future.

ACKNOWLEDGMENTS

B.P. would like to thank the Department of Science & Technology (Grant Nos. SB/FTP/PS-148/2013 and SR/S2/RJN-55/2012) for financial support. The authors are also grateful to the Ministry of Education, India for their financial support (Grant No. F.No. 5-5/2014-TS.Vll).

AUTHOR DECLARATIONS

Conflict of Interest

The authors have no conflict of interest to disclose.

DATA AVAILABILITY

The data that support the findings of the study are available from the corresponding author upon reasonable request.

REFERENCES

[1]J.-P. Correa-Baena, A. Abate, M. Saliba, W. Tress, T. J. Jacobsson, M. Grätzel, and A. Hagfeldt, Energy Environ. Sci. **10**, 710 (2017).
[2]J.-P. Correa-Baena, M. Saliba, T. Buonassisi, M. Grätzel, A. Abate, W. Tress, and A. Hagfeldt, Science **358**, 739 (2017).
[3]A. Mahapatra, S. Kumar, P. Kumar, and B. Pradhan, Mater.Today Chem. **23**, 100686 (2022).
[4]A. Kojima, K. Teshima, Y. Shirai, and T. Miyasaka, J. Am. Chem. Soc. **131**, 6050 (2009).
[5]See https://www.nrel.gov/pv/cell-efficiency.html for Solar Cell Efficiency Chart.
[6]A. K. Jena, A. Kulkarni, and T. Miyasaka, Chem. Rev. **119**, 3036 (2019).
[7]K. Nishimura, M. A. Kamarudin, D. Hirotani, K. Hamada, Q. Shen, S. Iikubo, T. Minemoto, K. Yoshino, and S. Hayase, Nano Energy **74**, 104858 (2020).
[8]T. Shi, H.-S. Zhang, W. Meng, Q. Teng, M. Liu, X. Yang, Y. Yan, H.-L. Yip, and Y.-J. Zhao, J. Mater. Chem. A **5**, 15124 (2017).
[9]S. Gupta, D. Cahen, and G. Hodes, J. Phys. Chem. C **122**, 13926 (2018).
[10]R. L. Milot, G. E. Eperon, T. Green, H. J. Snaith, M. B. Johnston, and L. M. Herz, J. Phys. Chem. Lett. **7**, 4178 (2016).
[11]F. Hao, C. C. Stoumpos, D. H. Cao, R. P. Chang, and M. G. Kanatzidis, Nat. Photonics **8**, 489 (2014).

[12]S. J. Lee, S. S. Shin, Y. C. Kim, D. Kim, T. K. Ahn, J. H. Noh, J. Seo, and S. I. Seok, J. Am. Chem. Soc. **138**, 3974 (2016).
[13]M. H. Kumar, S. Dharani, W. L. Leong, P. P. Boix, R. R. Prabhakar, T. Baikie, C. Shi, H. Ding, R. Ramesh, M. Asta, M. Graetzel, S.G. Mhaisalkar, and N. Mathews, Adv. Mater. **26**, 7122 (2014).
[14]Z. Zhao, F. Gu, Y. Li, W. Sun, S. Ye, H. Rao, Z. Liu, Z. Bian, and C. Huang, Adv. Sci. **4**, 1700204 (2017).
[15]S. Abdelaziz, A. Zekry, A. Shaker, and M. Abouelatta, Opt. Mater. **101**, 109738 (2020).
[16]N. K. Noel, S. D. Stranks, A. Abate, C. Wehrenfennig, S. Guarnera, A.-A. Haghighirad, A. Sadhanala, G. E. Eperon, S. K. Pathak, M. B. Johnston, A. Petrozza, L. M. Herz, and H. J. Snaith, Energy Environ. Sci. **7**, 3061 (2014).
[17]W. Ke and M. G. Kanatzidis, Nat. Commun. **10**, 965 (2019).
[18]Y. Raoui, H. Ez-Zahraouy, N. Tahiri, O. El Bounagui, S. Ahmad, and S. Kazim, Solar Energy **193**, 948 (2019).
[19]Q. Duan, J. Ji, X. Hong, Y. Fu, C. Wang, K. Zhou, X. Liu, H. Yang, and Z.-Y. Wang, Solar Energy **201**, 555 (2020).
[20]M. Burgelman, P. Nollet, and S. Degrave, Thin Solid Films **361–362**, 527 (2000).
[21]M. Kumar, A. Raj, A. Kumar, and A. Anshul, Opt. Mater. **108**, 110213 (2020).
[22]B. Smith, "Efficient lead-free perovskite solar cell" (2018); available at https://443.ece.illinois.edu/files/2018/09/SolarCellReportSmithWaterMarked.pdf
[23]J. A. Owolabi, M. Y. Onimisi, J. A. Ukwenya, A. B. Bature, and U. R. Ushiekpan, Am. J. Phys. Appl. **8**, 1 (2020).
[24]A. B. Coulibaly, S. O. Oyedele, and B. Aka, Model. Numer. Simul. Mater. Sci. **9**, 97 (2019).
[25]J. Madan, R. Pandey, and R. Sharma, Solar Energy **197**, 212 (2020).
[26]S. Li, P. Liu, L. Pan, W. Li, S.-E. Yang, Z. Shi, H. Guo, T. Xia, S. Zhang, and Y. Chen, Sol. Energy Mater. Sol. Cells **199**, 75 (2019).
[27]Y. H. Khattak, F. Baig, A. Shuja, S. Beg, and B. M. Soucase, Solar Energy **207**, 579 (2020).
[28]A. K. Singh, S. Srivastava, A. Mahapatra, J. K. Baral, and B. Pradhan, Opt. Mater. **117**, 111193 (2021).
[29]T. M. Koh, T. Krishnamoorthy, N. Yantara, C. Shi, W. L. Leong, P. P. Boix, A. C. Grimsdale, S. G. Mhaisalkar, and N. Mathews, J. Mater. Chem. A **3**, 14996 (2015).
[30]L. Lin, P. Li, L. Jiang, Z. Kang, Q. Yan, H. Xiong, S. Lien, P. Zhang, and Y. Qiu, Solar Energy **215**, 328 (2021).
[31]D. K. Maram, M. Haghighi, O. Shekoofa, H. Habibiyan, and H. Ghafoorifard, Solar Energy **213**, 1 (2021).
[32]V. A. Trukhanov, V. V. Bruevich, and D. Y. Paraschuk, Phys. Rev. B **84**, 205318 (2011).
[33]C. C. Stoumpos, C. D. Malliakas, and M. G. Kanatzidis, Inorg. Chem. **52**, 9019 (2013).
[34]S. S. Hussain, S. Riaz, G. A. Nowsherwan, K. Jahangir, A. Raza, M. J. Iqbal, I. Sadiq, S. M. Hussain, and S. Naseem, J. Renew. Energy **2021**, 1–12 (2021).
[35]S. Lin, B. Zhang, T.-Y. Lü, J.-C. Zheng, H. Pan, H. Chen, C. Lin, X. Li, and J. Zhou, ACS Omega **6**, 26689 (2021).
[36]M. A. Shafi, H. Ullah, S. Ullah, L. Khan, S. Bibi, and B. M. Soucase, Eng. Proc. **12**, 92 (2022).
[37]Z. Xiao, Z. Song, and Y. Yan, Adv. Mater. **31**, 1803792 (2019).
[38]Y. Zhou and Y. Zhao, Energy Environ. Sci. **12**, 1495 (2019).